J. Fluid Mech. (1991), *vol.* 231, *pp.* 417–437
Printed in Great Britain

Mass transport in three-dimensional water waves

By MOHAMED ISKANDARANI AND PHILIP L.-F. LIU
Joseph Defrees Hydraulics Laboratory, School of Civil and Environmental Engineering, Cornell University, Ithaca, NY 14853, USA

(Received 13 December 1990 and in revised form 15 March 1991)

A spectral scheme is developed to study the mass transport in three-dimensional water waves where the steady flow is assumed to be periodic in two horizontal directions. The velocity–vorticity formulation is adopted for the numerical solution, and boundary conditions for the vorticity are derived to enforce the no-slip conditions. The numerical scheme is used to calculate the mass transport under two intersecting wave trains; the resulting flow is reminiscent of the Langmuir circulation patterns. The scheme is then applied to study the steady flow in a three-dimensional standing wave.

1. Introduction

The objective of the present paper is to study the mass transport induced by three-dimensional water waves. These steady flows, although small in magnitude, play a significant role in the migration of particles and sediments. Dore (1976) derived the equations governing the mass transport outside the Stokes boundary layers. These equations describe the transport of the steady vorticity through vortex stretching and rotation, convection by the mean flow, and viscous diffusion. The ratio of the wave amplitude to the viscous length, δ, controls the balance between the diffusion, and the vortex stretching and convection. Diffusion dominates when δ is large; the governing equations can then be linearized by discarding the nonlinear terms. When δ is small, as is usually the case, the mass transport acquires a boundary-layer character. The complexity of the equations, and the limited computing power available in the past restricted previous numerical simulations to two-dimensional problems only.

In a previous paper, Iskandarani & Liu (1991) presented a spectral method for the solution of the two-dimensional mass transport equations in partially reflected waves. The scheme employed the stream function–vorticity formulation, and was based on a spectral expansion of the dependent variables. No stream function exists to describe three-dimensional flows. Their approach must be modified to study the mass transport induced by three-dimensional water waves.

A spectral method based on the velocity–vorticity formulation, where the unknowns are the three components of the steady velocity and vorticity vectors, is presented herein. The steady flows are periodic in the two horizontal directions. Spectral methods, which rely on Fourier expansions of the dependent variables, become an ideal choice to resolve the horizontal dependency of the flow. Chebyshev polynomial are chosen to resolve the vertical dependency. The advantages of the Fourier expansion are many. First, the Fourier functions ensure the periodicity of the flow in the horizontal directions, no boundary conditions are needed on the lateral boundaries. Second, the no-slip conditions on the tangential velocities can be

transformed analytically into constraints on the vorticity. Third, Chebyshev polynomials and Fourier functions can be fast Fourier transformed (FFT); the coefficients of the nonlinear terms in the equations can thus be computed efficiently with three-dimensional FFTs.

The solution procedure hinges on three key steps. The first step is the determination of the vorticity vector from the vorticity transport equation. The second step is the derivation of adequate boundary conditions on the vorticity at the boundaries where the tangential velocity components are prescribed. The third step is the integration of the vorticity vector to obtain the corresponding solenoidal velocity vector; this problem has been termed the Cauchy–Riemann problem (Fix & Rose 1985). The last two steps turn out to be intimately connected, and hold the key to the solution of the vorticity equation.

We begin by listing the governing equations and boundary conditions of the problem; these have been derived in the earlier work of Longuet-Higgins (1953), Dore (1976), and Liu (1977). We then examine the Cauchy–Riemann problem in §3, where we transform the no-slip conditions on the velocity to conditions on the vorticity. In §4, we present the numerical solution of the vorticity equation. The numerical scheme is then applied to study the mass transport under two intersecting wave trains, §5, and under a three-dimensional standing wave, §6.

2. Governing equations

The present formulation will be limited to flows where the first-order motion is harmonic in time; the Stokes drift and the Lagrangian velocities are then divergence free. The equation governing the transport of the second-order steady vorticity (Dore 1976) can be rewritten in the so-called rotational form

$$\delta^2 \nabla^2 \boldsymbol{\omega} + \nabla \times (\boldsymbol{v}_m \times \boldsymbol{\omega}) = 0, \tag{1}$$

in which the vectors $\boldsymbol{\omega}$ and $\boldsymbol{v}_m$ refer to the steady vorticity and to the mass transport velocity respectively. The mass transport velocity is a Lagrangian quantity, and is related to the Eulerian streaming velocity through (Longuet-Higgins 1953)

$$\boldsymbol{v}_m = \boldsymbol{v} + \boldsymbol{v}_s, \tag{2}$$

where $\boldsymbol{v}$ and $\boldsymbol{v}_s$ refer to the Eulerian streaming and the Stokes drift respectively. The vorticity is defined in terms of the Eulerian velocity

$$\boldsymbol{\omega} = \nabla \times \boldsymbol{v} \tag{3}$$

and the latter satisfies the continuity equation

$$\nabla \cdot \boldsymbol{v} = 0. \tag{4}$$

In this paper, we shall solve (1), (3), and (4) for the steady vorticity and Eulerian streaming velocity under three-dimensional small-amplitude waves. The first-order wave motion is assumed to be prescribed and periodic in both horizontal directions (x, y). The water depth is constant; the still water surface is at $z = 0$, and the seabed at $z = -h$. The vorticity components in the x-, y- and z-directions will be denoted by ω^x, ω^y and ω^z, and the velocity components by u, v and w. The subscript s will designate the components of the Stokes drift, while the superscripts s and b will refer to quantities evaluated on the surface and seabed respectively.

Using the existing theories, the Eulerian streaming and the steady vorticity can be readily obtained inside the Stokes' boundary layers adjacent to the free surface and the seabed (Longuet-Higgins 1953; Liu 1977). The boundary conditions for the steady flow outside the Stokes layers ($-h \leqslant z \leqslant 0$) can be found by evaluating the Stokes layer solutions at the outer edge of the boundary layers. Thus, the steady horizontal vorticity components are prescribed on the free surface

$$\omega^x(x, y, z = 0) = \omega^{x,\mathrm{s}}(x, y), \quad \omega^y(x, y, z = 0) = \omega^{y,\mathrm{s}}(x, y), \tag{5}$$

and the horizontal Eulerian streaming velocity components are prescribed on the seabed

$$u(x, y, z = -h) = u^{\mathrm{b}}(x, y), \quad v(x, y, z = -h) = v^{\mathrm{b}}(x, y). \tag{6}$$

The vertical velocity component vanishes on the seabed,

$$w(x, y, z = -h) = 0, \tag{7}$$

and the free surface is a material surface, hence

$$w(x, y, z = 0) = -w_{\mathrm{s}}(x, y, z = 0) = w^{\mathrm{s}}(x, y). \tag{8}$$

Furthermore, because of its definition, (3), the vorticity must be solenoidal, particularly at the seabed and free surface,

$$\nabla \cdot \boldsymbol{\omega} = 0 \quad \text{at} \quad z = 0, -h. \tag{9}$$

Because the mass transport is periodic and the Chebyshev polynomials are defined over the interval $[-1, 1]$, we introduce the new independent variables $\xi = k_x x$, $\zeta = k_y y$ and $\eta = (2/h) z + 1$, where $2\pi/k_x$ and $2\pi/k_y$ are the wavelengths of the steady motion in the x- and y-directions respectively. Two expansions of the dependent variables are employed. The first is a Fourier expansion whose coefficients depend on the vertical coordinate:

$$f(\xi, \zeta, \eta) = \sum_{n=-N}^{N} \sum_{m=-M}^{M} f_{m,n}(\eta)\, \mathrm{e}^{\mathrm{i}m\zeta}\, \mathrm{e}^{\mathrm{i}n\xi},$$

where f is any one of the steady velocity or vorticity components; this expansion is mainly used in the integration of the Cauchy–Riemann equations. Note that since f is real, we have $f_{-m,-n} = f^*_{m,n}$ where the asterisk denotes a complex conjugate; it is thus sufficient to focus on the modes $m = 0, 1, \ldots, M$, and $n = 0, \pm 1, \ldots, \pm N$. Variables with two subscripts, like $f_{m,n}(\eta)$, refer to the coefficients of the *Fourier* expansion of the function $f(\xi, \zeta, \eta)$. The second expansion is the Chebyshev expansion of each Fourier coefficient

$$f_{m,n}(\eta) = \sum_{l=0}^{L} f_{l,m,n}\, T_l(\eta).$$

Its coefficients, $f_{l,m,n}$, are referred to as the *Fourier–Chebyshev* coefficients of the function $f(\xi, \zeta, \eta)$.

3. Cauchy–Riemann problem

The three-dimensional Cauchy–Riemann problem consists of integrating the vorticity definition, equation (3), to find a velocity that satisfies (4), and whose

normal component is prescribed at the boundary (7) and (8). The existence and uniqueness of the solution to this system of equations is guaranteed, provided that the vorticity vector $\boldsymbol{\omega}$ is solenoidal (Fix & Rose 1985). Fasel (1976) and Gatski, Grosch & Rose (1989) presented different approaches for the solution of the Cauchy–Riemann problem. The former solves three Poisson equations for each component of the velocity, while the latter consider the Cauchy–Riemann problem as a set of first-order PDEs. In the present work, the Fourier decomposition reduces the partial differential equations to ordinary differential equations that can be integrated analytically.

Applying the Fourier decomposition to (3), (4), (7) and (8), each Fourier mode (m, n) should satisfy the following set of equations:

$$\omega^x_{m,n} = \mathrm{i}mk_y w_{m,n} - \frac{2}{h}\frac{\mathrm{d}v_{m,n}}{\mathrm{d}\eta}, \tag{10}$$

$$\omega^y_{m,n} = \frac{2}{h}\frac{\mathrm{d}u_{m,n}}{\mathrm{d}\eta} - \mathrm{i}nk_x w_{m,n}, \tag{11}$$

$$\omega^z_{m,n} = \mathrm{i}nk_x v_{m,n} - \mathrm{i}mk_y u_{m,n}, \tag{12}$$

$$\mathrm{i}nk_x u_{m,n} + \mathrm{i}mk_y v_{m,n} + \frac{2}{h}\frac{\mathrm{d}w_{m,n}}{\mathrm{d}\eta}, \tag{13}$$

$$w_{m,n}(\eta = -1) = 0, \quad w_{m,n}(\eta - 1) = w^{\mathrm{s}}_{m,n}. \tag{14}$$

Again, we emphasize that the vorticity has to be solenoidal for the above system of equations to hold:

$$\mathrm{i}nk_x \omega^x_{m,n} + \mathrm{i}mk_y \omega^y_{m,n} + \frac{2}{h}\frac{\mathrm{d}\omega^z_{m,n}}{\mathrm{d}\eta} = 0. \tag{15}$$

Rewriting (10) and (11) as

$$\frac{\mathrm{d}u_{m,n}}{\mathrm{d}\eta} = \tfrac{1}{2}h(\mathrm{i}nk_x w_{m,n} + \omega^y_{m,n}), \tag{16}$$

$$\frac{\mathrm{d}v_{m,n}}{\mathrm{d}\eta} = \tfrac{1}{2}h(\mathrm{i}mk_y w_{m,n} - \omega^x_{m,n}) \tag{17}$$

and differentiating the continuity equation, (13), with respect to η, we can eliminate the horizontal velocity components from the resulting equations. Thus, a second-order ODE for the vertical component of the velocity is found:

$$\frac{\mathrm{d}^2 w_{m,n}}{\mathrm{d}\eta^2} - \lambda^2 w_{m,n} + \tfrac{1}{4}h^2[\mathrm{i}nk_x \omega^y_{m,n} - \mathrm{i}mk_y \omega^x_{m,n}] = 0, \tag{18}$$

$$\lambda^2 = \tfrac{1}{4}h^2(n^2k_x^2 + m^2k_y^2). \tag{19}$$

If the vorticity field is given, the above equation can be solved analytically for the vertical velocity component $w_{m,n}$. Equations (16) and (17) can then be integrated for the horizontal velocity components. Two different solutions for $w_{m,n}$ emerge according to whether λ is zero or not, the case $\lambda \neq 0$ is treated first.

3.1. $\lambda \neq 0$

The solution to (16)–(18) subject to boundary conditions (14) is

$$w_{m,n}(\eta) = \frac{h^2}{4\lambda}\int_{-1}^{\eta}[ink_x\omega^y_{m,n}(r) - imk_y\omega^x_{m,n}(r)]\sinh\lambda(r-\eta)\,dr + \frac{h}{2\lambda}B\sinh\lambda(\eta+1), \tag{20}$$

$$u_{m,n}(\eta) = C_u + \frac{h}{2}\int_{-1}^{\eta}[\omega^y_{m,n}(r) + ink_x w_{m,n}(r)]\,dr, \tag{21}$$

$$v_{m,n}(\eta) = C_v - \frac{h}{2}\int_{-1}^{\eta}[\omega^x_{m,n}(r) - imk_y w_{m,n}(r)]\,dr, \tag{22}$$

where B is given by

$$B = \frac{2\lambda}{h}\frac{w^s_{m,n}}{\sinh 2\lambda} - \frac{h}{2}\int_{-1}^{1}[ink_x\omega^y_{m,n}(\eta) - imk_y\omega^x_{m,n}(\eta)]\frac{\sinh\lambda(\eta-1)}{\sinh 2\lambda}d\eta, \tag{23}$$

and C_u and C_v are two unknown constants of integration that give the horizontal velocity components on the seabed ($\eta = -1$).

To determine C_u and C_v, we substitute the expressions for the velocity components, (20), (21) and (22), in (13) and (12) to obtain the following equations:

$$ink_x C_u + imk_y C_v + B = 0, \tag{24}$$

$$ink_x C_v - imk_y C_u = \omega^z_{m,n}(\eta = -1) = \omega^{z,b}_{m,n}, \tag{25}$$

where B is given in (23). Equations (24) and (25) can be solved for C_u and C_v when $\lambda \neq 0$:

$$C_u = \frac{h^2}{4\lambda^2}(ink_x B + imk_y\omega^{z,b}_{m,n}), \tag{26}$$

$$C_v = \frac{h^2}{4\lambda^2}(imk_y B - ink_x\omega^{z,b}_{m,n}). \tag{27}$$

So far, C_u and C_v are two integration constants not related to any prescribed velocity on the seabed, and solely determined by the solenoidal vorticity vector, the vertical velocity at the boundary, and the continuity requirement. However, in the present problem, the horizontal velocity components on the seabed are known; C_u and C_v should be equal to the prescribed velocity $u^b_{m,n}$ and $v^b_{m,n}$ in (6). These are requirements that impose constraints on the vorticity field. Setting C_u and C_v equal to $u^b_{m,n}$ and $v^b_{m,n}$ in (24) and (25), solving for $\omega^{z,b}_{m,n}$ and B, and equating the resultant expression for B to the expression in (23), we obtain the following relations:

$$\omega^z_{m,n}(\eta = -1) = ink_x v^b_{m,n} - imk_y u^b_{m,n}, \tag{28}$$

$$\int_{-1}^{1}[ink_x\omega^y_{m,n}(\eta) - imk_y\omega^x_{m,n}(\eta)]\frac{\sinh\lambda(\eta-1)}{\sinh 2\lambda}d\eta = \frac{4\lambda}{h^2}\frac{w^s_{m,n}}{\sinh 2\lambda} + \frac{2}{h}[ink_x u^b_{m,n} + imk_y v^b_{m,n}]. \tag{29}$$

We reiterate that (28) and (29) are the conditions needed on the vorticity to enforce the values of the horizontal velocity components on the seabed.

3.2. $\lambda = 0$

The analysis in the previous section is correct as long as $\lambda \neq 0$. When $\lambda = 0$, (12) gives

$$\omega^z_{0,0} = 0. \tag{30}$$

Hence the spatial mean of the vertical vorticity component is identically zero. Moreover, the continuity equation, (13), implies that $w_{0,0} = 0$ since the vertical velocity vanishes on the seabed. The horizontal velocities can be obtained by integrating (10) and (11):

$$u_{0,0} = C_u + \frac{h}{2}\int_{-1}^{\eta} \omega^y_{0,0}(r)\,\mathrm{d}r, \quad v_{0,0} = C_v - \frac{h}{2}\int_{-1}^{\eta} \omega^x_{0,0}(r)\,\mathrm{d}r, \tag{31}$$

where C_u and C_v are again two constants of integration. Unlike the case $\lambda \neq 0$, the continuity equation, the definition of the z-component of the vorticity, and the solenoidality of the vorticity vector are trivially satisfied and cannot be used to determine C_u and C_v.

Defining q_x and q_y as the averaged horizontal flux components (per unit width) in the x- and y-directions respectively,

$$q_x = \frac{h}{2}\int_{-1}^{1} u_{0,0}(\eta)\,\mathrm{d}\eta, \quad q_y = \frac{h}{2}\int_{-1}^{1} v_{0,0}(\eta)\,\mathrm{d}\eta, \tag{32}$$

we substitute the expressions for $u_{0,0}$ and $v_{0,0}$, (31), in the above definitions to get

$$q_x = hC_u - \frac{h^2}{4}\int_{-1}^{1} \omega^y_{0,0}(\eta)\,(\eta - 1)\,\mathrm{d}\eta, \tag{33}$$

$$q_y = hC_v + \frac{h^2}{4}\int_{-1}^{1} \omega^x_{0,0}(\eta)\,(\eta - 1)\,\mathrm{d}\eta. \tag{34}$$

If the averaged horizontal flux components q_x and q_y are given, we can find C_u and C_v from the above equations. On the other hand, if both the horizontal velocity components on the seabed and the horizontal flux components are prescribed, the zeroth mode of the vorticity vector must satisfy

$$\int_{-1}^{1} \omega^x_{0,0}(\eta)\,(\eta - 1)\,\mathrm{d}\eta = \frac{4}{h^2}(q_y - hv^{\mathrm{b}}_{0,0}), \tag{35}$$

$$\int_{-1}^{1} \omega^y_{0,0}(\eta)\,(\eta - 1)\,\mathrm{d}\eta = -\frac{r}{h^2}(q_x - hu^{\mathrm{b}}_{0,0}). \tag{36}$$

The last two equations are the boundary conditions needed on the zeroth Fourier modes of the vorticity to impose the horizontal velocity components on the seabed. As in the two-dimensional case (Iskandarani & Liu 1991), we will assume that a return current has been established so that the average fluxes of particles in the x- and y-directions are equal to zero. Hence,

$$q_x = -\frac{h}{2}\int_{-1}^{1} (u_{\mathrm{s}})_{0,0}(\eta)\,\mathrm{d}\eta, \tag{37}$$

$$q_y = -\frac{h}{2}\int_{-1}^{1} (v_{\mathrm{s}})_{0,0}(\eta)\,\mathrm{d}\eta, \tag{38}$$

where $(u_s)_{0,0}$ and $(v_s)_{0,0}$ denote the zero Fourier mode of the Stokes drift in the x- and y-directions respectively.

We have completed the solution of the Cauchy–Riemann problem, and derived analytical expressions for the Fourier coefficients of the velocity in terms of the Fourier coefficients of the vorticity. The expressions for the Fourier–Chebyshev coefficients can be found in Iskandarani (1991). Moreover, we have derived the boundary conditions necessary to solve the vorticity equations for all Fourier modes, and we now turn to the numerical solution of the vorticity equations.

4. Vorticity equations

Following the approach of the two-dimensional formulation (Iskandarani & Liu 1991), we introduce a transient term in (1) to allow the nonlinearities to develop gradually. The component form of (1) becomes

$$\frac{\partial \omega^x}{\partial \tau} = \tfrac{1}{4}h^2\nabla^2\omega^x + \frac{h^2}{4\delta^2}\left[k_y\frac{\partial(u_m\omega^y - v_m\omega^x)}{\partial\zeta} - \frac{2}{h}\frac{\partial(w_m\omega^x - u_m\omega^z)}{\partial\eta}\right], \tag{39}$$

$$\frac{\partial \omega^y}{\partial \tau} = \tfrac{1}{4}h^2\nabla^2\omega^y + \frac{h^2}{4\delta^2}\left[\frac{2}{h}\frac{\partial(v_m\omega^z - w_m\omega^y)}{\partial\eta} - k_x\frac{\partial(u_m\omega^y - v_m\omega^x)}{\partial\xi}\right], \tag{40}$$

$$\frac{\partial \omega^z}{\partial \tau} = \tfrac{1}{4}h^2\nabla^2\omega^z + \frac{h^2}{4\delta^2}\left[k_x\frac{\partial(w_m\omega^x - u_m\omega^z)}{\partial\xi} - k_y\frac{\partial(v_m\omega^z - w_m\omega^y)}{\partial\zeta}\right], \tag{41}$$

$$\nabla^2 = k_x^2\frac{\partial^2}{\partial\xi^2} + k_y^2\frac{\partial^2}{\partial\zeta^2} + \frac{4}{h^2}\frac{\partial^2}{\partial\eta^2}. \tag{42}$$

We adopt the Galerkin–Tau method (Canuto *et al.* 1988) to find the numerical solution of (39)–(41). Applying the Fourier–Chebyshev expansions to (39)–(41) yields the following system of equations for the Fourier–Chebyshev coefficients:

$$\frac{\mathrm{d}\omega^x_{l,m,n}}{\mathrm{d}\tau} = \omega^{x(2)}_{l,m,n} - \lambda^2\omega^x_{l,m,n} + f^x_{l,m,n}, \tag{43}$$

$$\frac{\mathrm{d}\omega^y_{l,m,n}}{\mathrm{d}\tau} = \omega^{y(2)}_{l,m,n} - \lambda^2\omega^y_{l,m,n} + f^y_{l,m,n}, \tag{44}$$

$$\frac{\mathrm{d}\omega^z_{l,m,n}}{\mathrm{d}\tau} = \omega^{z(2)}_{l,m,n} - \lambda^2\omega^z_{l,m,n} + f^z_{l,m,n}, \tag{45}$$

$$\lambda = \tfrac{1}{2}h(n^2k_x^2 + m^2k_y^2)^{\frac{1}{2}},$$

$$l = 0, 1, 2, \ldots, L-2, \quad m = 0, 1, 2, \ldots, M, \quad n = 0, \pm1, \pm2, \ldots, \pm N.$$

The $f_{l,m,n}$ are the coefficients of the vector components of the nonlinear terms in (39)–(41), i.e.

$$\sum_{l=0}^{L}\sum_{m=-M}^{M}\sum_{n=-N}^{N} f^x_{l,m,n}\phi_{l,m,n} = \frac{h^2}{4\delta^2}\left[k_y\frac{\partial(u_m\omega^y - v_m\omega^x)}{\partial\zeta} - \frac{2}{h}\frac{\partial(w_m\omega^x - u_m\omega^z)}{\partial\eta}\right],$$

$$\sum_{l=0}^{L}\sum_{m=-M}^{M}\sum_{n=-N}^{N} f^y_{l,m,n}\phi_{l,m,n} = \frac{h^2}{4\delta^2}\left[\frac{2}{h}\frac{\partial(v_m\omega^z - w_m\omega^y)}{\partial\eta} - k_x\frac{\partial(u_m\omega^y - v_m\omega^x)}{\partial\xi}\right],$$

$$\sum_{l=0}^{L}\sum_{m=-M}^{M}\sum_{n=-N}^{N} f^z_{l,m,n}\phi_{l,m,n} = \frac{h^2}{4\delta^2}\left[k_x\frac{\partial(w_m\omega^x - u_m\omega^z)}{\partial\xi} - k_y\frac{\partial(v_m\omega^z - w_m\omega^y)}{\partial\zeta}\right],$$

with $\phi_{l,m,n}(\xi,\zeta,\eta) = T_l(\eta)\,\mathrm{e}^{\mathrm{i}m\zeta}\mathrm{e}^{\mathrm{i}n\xi}$ which can be viewed as the shape functions. In (43)–(45), $\omega^{k(2)}_{l,m,n}$ denotes the Fourier–Chebyshev coefficients of the second derivative with respect to η of the k-component ($k = x, y, z$) of the vorticity vector, i.e.

$$\omega^{k(2)}_{l,m,n} = \frac{1}{c_l}\sum_{p=l+2,\,2}^{L} p(p^2-l^2)\,\omega^{k}_{p,m,n},$$

where $c_0 = 2$, and $c_l = 1$ for $l \geqslant 1$.

The boundary conditions (5) prescribing the x- and y-components of the vorticity at the free surface are rewritten in terms of the Fourier–Chebyshev coefficients

$$\sum_{l=0}^{L} \omega^{x}_{l,m,n} = \omega^{x,\mathrm{s}}_{m,n}, \tag{46}$$

$$\sum_{l=0}^{L} \omega^{y}_{l,m,n} = \omega^{y,\mathrm{s}}_{m,n}. \tag{47}$$

The enforcement of the tangential velocity components at the seabed requires, when $\lambda \neq 0$, the two constraints

$$\sum_{l=0}^{L} (-1)^l \omega^{z}_{l,m,n} = \mathrm{i}nk_x v^{\mathrm{b}}_{m,n} - \mathrm{i}mk_y u^{\mathrm{b}}_{m,n}, \tag{48}$$

$$\sum_{l=0}^{L} [\mathrm{i}nk_x \omega^{y}_{l,m,n} - \mathrm{i}mk_y \omega^{x}_{l,m,n}] S_{l,m,n} = \frac{4\lambda}{h^2}\frac{w^{\mathrm{s}}_{m,n}}{\sinh 2\lambda} + \frac{2}{h}[\mathrm{i}nk_x u^{\mathrm{b}}_{m,n} + \mathrm{i}mk_y v^{\mathrm{b}}_{m,n}], \tag{49}$$

with
$$S_{l,m,n} = \int_{-1}^{1} T_l(\eta)\frac{\sinh\lambda(\eta-1)}{\sinh 2\lambda}\,\mathrm{d}\eta,$$

where we have substituted the Chebyshev expansions into the left-hand sides of (28) and (29). The $S_{l,m,n}$ can be evaluated by expanding the hyperbolic sine in a Chebyshev series (Iskandarani & Liu 1991).

When $\lambda = 0$, the two constraints to enforce $u^{\mathrm{b}}_{0,0}$ and $v^{\mathrm{b}}_{0,0}$ on the seabed are given by (35) and (36). In terms of the Fourier–Chebyshev coefficients, these constraints become

$$\sum_{l=0}^{L} \omega^{x}_{l,0,0} S_{l,0,0} = \frac{4}{h^2}(q_y - hv^{\mathrm{b}}_{0,0}), \tag{50}$$

$$\sum_{l=0}^{L} \omega^{y}_{l,0,0} S_{l,0,0} = -\frac{4}{h^2}(q_x - hu^{\mathrm{b}}_{0,0}), \tag{51}$$

where
$$S_{l,0,0} = \int_{-1}^{1} T_l(\eta)(\eta-1)\,\mathrm{d}\eta = \begin{cases} 2/(l^2-1) & (l \text{ even}) \\ -2/(l^2-4) & (l \text{ odd}). \end{cases}$$

Finally, the solenoidality of the vorticity field at the surface and the seabed gives the following conditions:

$$\sum_{l=0}^{L} l^2 \omega^{z}_{l,m,n} = -\tfrac{1}{2}h(\mathrm{i}nk_x \omega^{x,\mathrm{s}}_{m,n} + \mathrm{i}mk_y \omega^{y,\mathrm{s}}_{m,n}), \tag{52}$$

$$\sum_{l=0}^{L} (-1)^l [\mathrm{i}nk_x \omega^{x}_{l,m,n} + \mathrm{i}mk_y \omega^{y}_{l,m,n}] = -\frac{2}{h}\sum_{l=0}^{L} (-1)^{l-1} l^2 \omega^{z}_{l,m,n}. \tag{53}$$

Equations (43)–(53) are a system of $3(2N+1)(M+1)(L+1)$ nonlinear ordinary differential equations for the $6(2N+1)(M+1)(L+1)$ Fourier–Chebyshev coefficients of the vorticity and velocity. The Cauchy–Riemann problem supplies the remaining half of the equations. The nonlinear terms in the governing equations link all the Fourier–Chebyshev modes of the velocity and vorticity components. The boundary conditions on the other hand are linear, and (49) and (53) couple the vorticity components of each Fourier mode only.

As in the two-dimensional case (Iskandarani & Liu 1991), the problem is linearized by approximating the nonlinear terms with information from a previous time step. The system of equations (43)–(45) can then be divided into a $(2N+1)(M+1)$ independent sets of ODEs for each Fourier mode (m, n). Each set involves only the $3(L+1)$ Chebyshev modes of the vorticity vector. Moreover (45), subject to (48) and (52), determines $\omega^z_{l,m,n}$ independently of the x and y vorticity components. Equations (43) and (44), with conditions (46), (47), (49) and (53), are then solved simultaneously for $\omega^x_{l,m,n}$ and $\omega^y_{l,m,n}$ when $\lambda \neq 0$. Notice that when either m or n is zero, the x- and y-components of the vorticity can be solved separately. In the special case where $m = n = 0$, the vertical component of the vorticity is identically zero, $\omega^x_{l,m,n}$ is the solution to (43), (46) and (50), and $\omega^y_{l,m,n}$ to (44), (47) and (51).

Finite differences are used for the time integration of (43)–(45). The nonlinear terms in the equations are integrated explicitly using a second-order Runge–Kutta scheme, while the viscous term is integrated implicitly for numerical stability. The nonlinear terms are computed efficiently using three-dimensional fast Fourier transforms (Gottlieb & Orszag 1977), and the $\frac{3}{2}$ rule is implemented to remove the aliasing errors. A major advantage of the present scheme is that it maintains a solenoidal vorticity field provided that the initial vorticity is solenoidal. Also, the velocity field satisfies the continuity equation at all times because of the Cauchy–Riemann problem.

5. Mass transport in intersecting wave trains

The numerical scheme presented in the previous sections will be used to compute the mass transport under two progressive waves travelling in different directions. If the angle between the two waves is 2θ, and the x-axis is along the median, the free-surface displacement can be described by

$$\zeta_f = \cos \kappa_y y \cos(\kappa_x x - t), \quad (\kappa_x, \kappa_y) = \kappa(\cos\theta, \sin\theta) \tag{54}$$

and has the shape of a wave progressing in the x-direction with amplitude that varies sinusoidally in the y-direction. The antinodes are located at $\zeta = 2n\pi$, while the nodes are at $\zeta = (2n+1)\pi, n = 0, 1, \ldots$. The wavenumber, κ, is given by the dispersion relation

$$\beta = \frac{\sigma^2}{g\bar{k}} = \kappa \tanh \kappa h,$$

where σ is the frequency of the wave, g the gravitational acceleration, h the water depth, and $\bar{k}$ a typical wavenumber in the problem. In our example, we will specify κ and h; β will be determined from the dispersion relation.

To find the mass transport, we must calculate the Stokes drift, the steady streaming on the seabed, and the components of the steady vorticity at the surface. The derivation of these terms can be found in the work of Longuet-Higgins (1953),

Hunt & Johns (1963) and Liu (1977); only the results will be listed here. The Stokes drift is given by

$$u_s = \frac{\kappa^3 \cos\theta}{8\beta^2 \cosh^2 \kappa h}[(\cos^2\theta \cosh 2\kappa(z+h) - \sin^2\theta)(e^{-ik_y y} + e^{ik_y y}) + 2\cosh 2\kappa(z+h)], \tag{55}$$

$$v_s = 0, \tag{56}$$

$$w_s = 0, \tag{57}$$

where $k_x = 2\kappa_x$, and $k_y = 2\kappa_y$. The horizontal vorticity at the surface is

$$\omega^{x,s} = 0, \tag{58}$$

$$\omega^{y,s} = \frac{-\kappa^4 \sinh 2\kappa h \cos\theta}{4\beta^2 \cosh^2 \kappa h}[\cos^2\theta\, e^{-ik_y y} + 2 + \cos^2\theta\, e^{ik_y y}], \tag{59}$$

and the steady streaming at the seabed is

$$u^b = \frac{\kappa^3 \cos\theta}{16\beta^2 \cosh^2 \kappa h}[3e^{-ik_y y} + 6 + 3e^{ik_y y}], \tag{60}$$

$$v^b = \frac{\kappa^3 \sin\theta(1+2\sin^2\theta)}{16\beta^2 \cosh^2 \kappa h}[-ie^{-ik_y y} + ie^{ik_y y}]. \tag{61}$$

The zeroth Fourier mode requires information about the net flux in the x- and y-directions. Both are assumed to be zero, and the Eulerian flux must then be equal and opposite to the integral of the Stokes drift along the vertical; hence, we obtain the following expressions for q_x and q_y:

$$q_x = \frac{-\kappa^2 \sinh 2\kappa h \cos\theta}{2\beta^2 \cosh^2 \kappa h}, \tag{62}$$

$$q_y = 0. \tag{63}$$

In this particular example, the mass transport is uniform in the x-direction as the boundary conditions do not depend on the x-coordinate. Hence, all the coefficients of the Fourier–Chebyshev modes ($0 \leqslant l \leqslant L, 0 \leqslant m \leqslant M, 1 \leqslant |n| \leqslant N$) are zero, and one needs to concentrate on the Fourier–Chebyshev modes ($0 \leqslant l \leqslant L, 0 \leqslant m \leqslant M, 0$) only.

The first set of experiments held the angle θ constant at 45°, while δ was given the successive values 10^4, 0.1, and 0.05. Figure 1 shows the variations of the three mass transport velocity components, u_m, v_m and w_m in the (y,z)-plane for the viscous limit $\delta = 10^4$. In this case, the problem is linear; this is reflected in the transverse sinusoidal variations of the three velocity components. The transverse horizontal coordinate y has been normalized with the wavenumber k_y; the figures focus on half a wavelength only; the flow in the remaining half wavelength can be deduced from symmetry. Figure (1*c*) shows the variation of the vertical velocity, w_m. It is positive throughout the depth for $0 \leqslant \zeta \leqslant \frac{1}{2}\pi$, and negative for $\frac{1}{2}\pi \leqslant \zeta \leqslant \pi$. The particles are hence rising gently near the antinode, and sinking near the node. The horizontal velocity u_m is larger in magnitude than the vertical velocity. It is forward in the whole depth under the antinode with maximum value at the surface. As we move away from the antinode, u_m decreases continuously until the flow becomes backward near the node. Near the seabed however, u_m is always positive. The y velocity

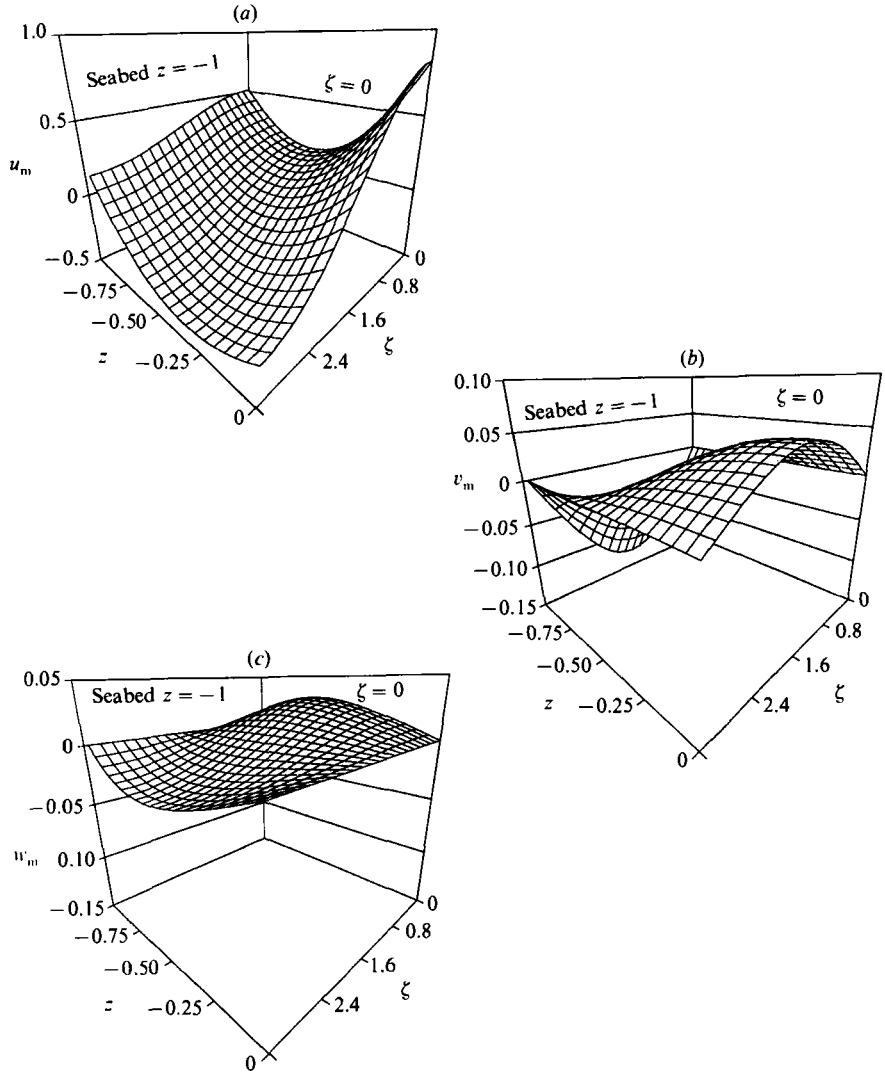

FIGURE 1. Mass transport velocity for $\theta = 45°$, $h = 1.0$, and $\delta = 10^4$. (*a*) u_m, (*b*) v_m, (*c*) w_m.

component, v_m, is shown in figure (1*b*). It is positive on the free surface, with particles moving away from the antinode towards the node; the opposite trend can be seen near the seabed. Along the lines $\zeta = 0, \pi$, v_m is identically zero.

When δ is 0.1, figure 2, new features that are usually associated with Langmuir circulation appear (Leibovich 1983). The picture for the horizontal velocity component, u_m, remains more or less the same, with a decrease in the maximum forward velocity at the free surface. The new features of the flow are mainly in the y- and z-components of the velocity. The flow of particles near the surface is now opposite to that found in the viscous limit: the particles are drifting away from the nodes towards the antinodes. Under the node and antinode, v_m is zero; it is negative on the surface and it reaches its maximum negative value close to the antinode. Below mid-depth, v_m is positive and the drift is toward the node. The most dramatic features are in the vertical velocity w_m, figure (2*c*). The gentle upwelling under the

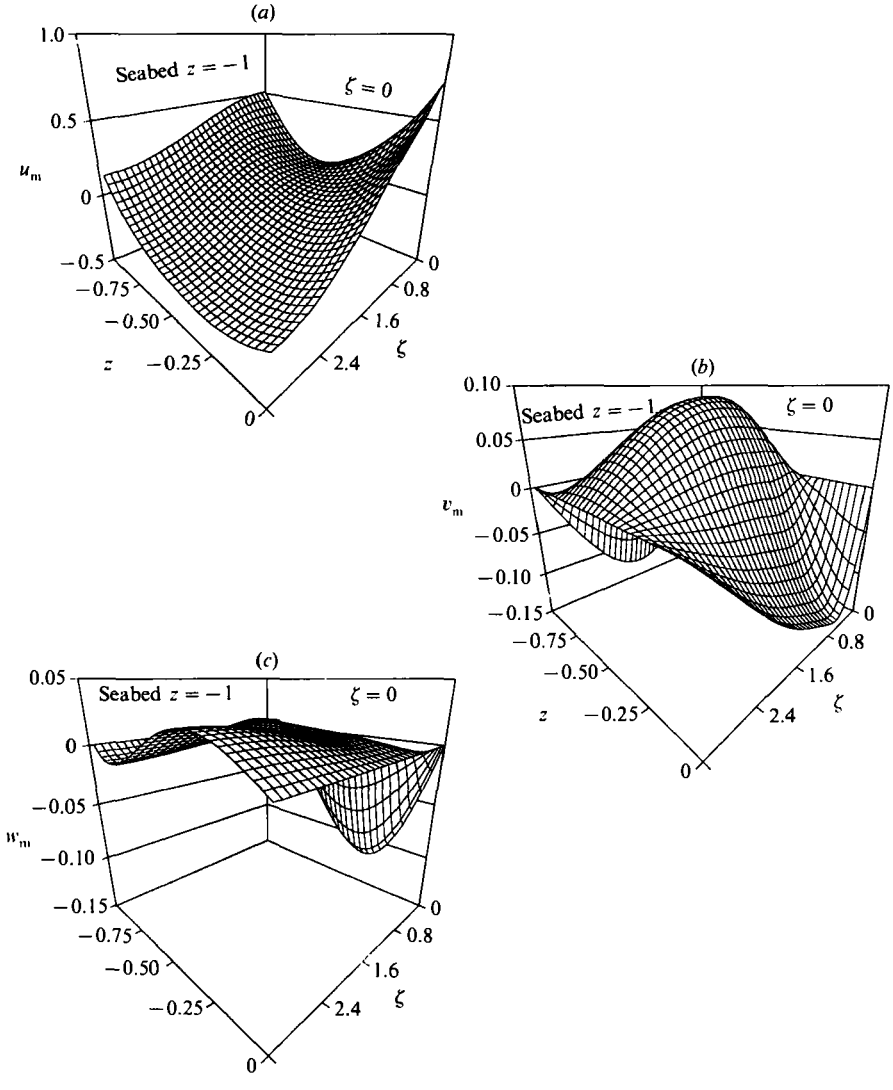

FIGURE 2. Mass transport velocity for $\theta = 45°$, $h = 1.0$, and $\delta = 0.1$: (*a*) u_m, (*b*) v_m, (*c*) w_m.

antinode has now turned into a strong downwelling in the upper part of the flow; in the lower part, near the seabed, the flow is upward. The magnitude of the vertical velocity in the upper part has increased to become of the same order as u_m. The region of strong downwelling is limited to the immediate neighbourhood of the antinode. Particles in the upper and lower part of the depth drift towards the level of zero vertical velocity; those that are immediately under the antinodes remain in the same plane, as the y-component of the velocity is zero. Away from the antinode, and in the upper part of the depth, the fluid is rising to the surface, while near the bottom it is drawn towards the seabed. Figure 3 shows vector diagrams of the projection of the mass transport velocity on the planes $\zeta = 0, \frac{1}{2}\pi, \pi$. Since there is no transverse velocity component at the node and antinode, figures (3*a*) and (3*c*) give the total velocity vector. In the former, the particles converge towards the level $z = -0.8$, while in the latter they diverge from $z = -0.75$. Midway between the node

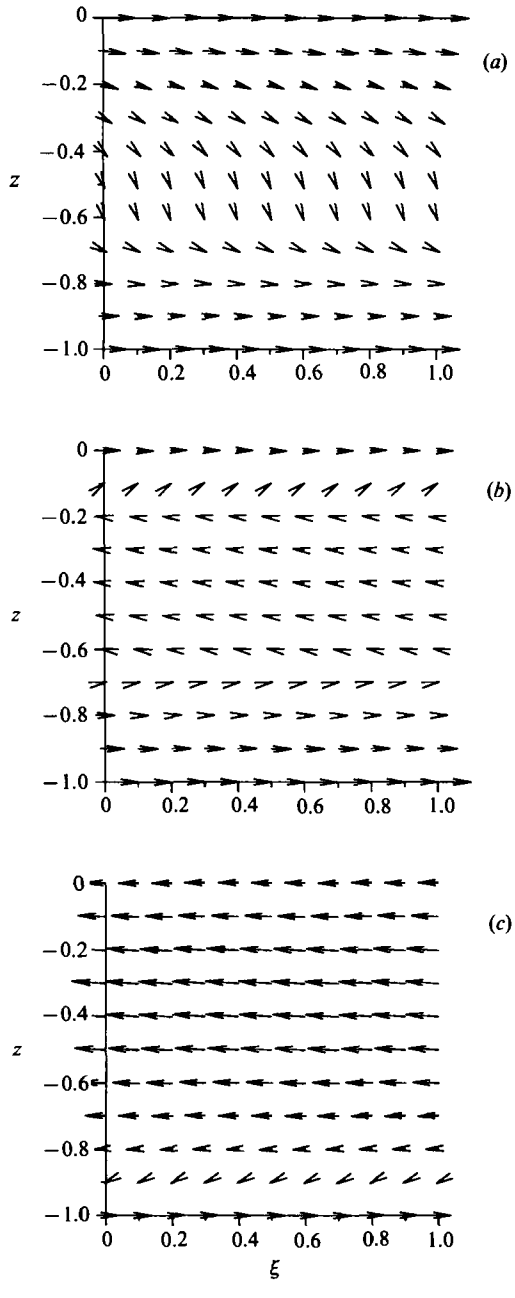

FIGURE 3. Projection of mass transport velocity on plane (*a*) $\zeta = 0$, (*b*) $\zeta = \frac{1}{2}\pi$ and (*c*) $\zeta = \pi$ for $\theta = 45°$, $h = 1.0$, and $\delta = 0.1$.

and antinode, figure (3*b*), fluid is rising towards the surface while moving forward near the surface and seabed; the flow is backward in between. Figure 4 is a projection of the velocity vector on the plane $\xi = 0$. Two counter-rotating vortices occupy the upper and lower part of the depth. The lower vortex is confined to the proximity of the seabed, and its centre is in the middle of the flow region. The upper vortex is larger, with its centre close to the antinode of the surface. Figures 5(*a*) and 5(*b*) show

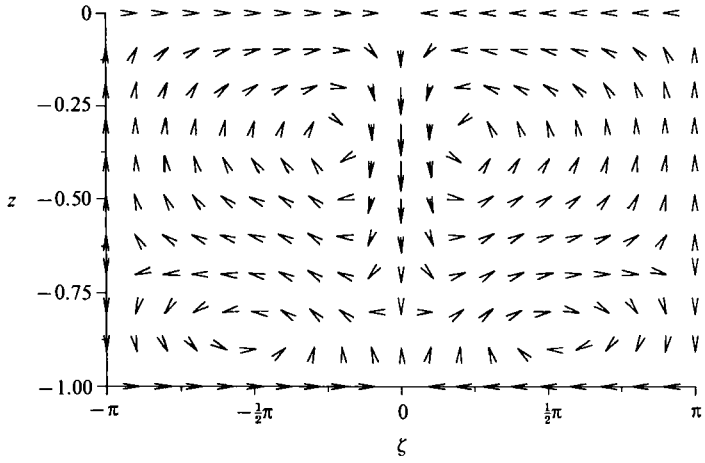

FIGURE 4. Projection of mass transport velocity on plane $\xi = 0$ for $\theta = 45°$, $h = 1.0$ and $\delta = 0.1$.

the paths of particles in the lower and upper vortex. In the lower vortex, the particle moves forward (in the direction of wave propagation) in a right-hand spiral while remaining close to the seabed. The motion in the upper vortex is more complex. The particle moves forward when it sinks near the antinode, and backward when it rises next to the nodal line; when the particle returns to its initial elevation, the net movement is a backward drift in the x direction. Figure (5c) is the trajectory of a fluid particle on the surface where the vertical drift is zero. Away from the nodes, fluid at the surface is entrained towards the antinodes, and the particles accumulating there form parallel streaklines that move in the direction of wave propagation.

The value of δ was decreased further to 0.05. Most of the general features reported for the $\delta = 0.1$ remained unchanged. The effects of the angle θ on the mass transport was studied by decreasing θ from 45° to 30° and 15°, and keeping $\delta = 0.1$. In general, the downwelling near the antinode becomes stronger and it becomes narrower as the two waves become more aligned; the upwelling velocity becomes smaller and spreads to a larger region. The features are similar to those observed for $\theta = 45°$, and will not be reported here. The details are given in Iskandarani (1991).

In his investigations on Langmuir circulation, Leibovich (1977) studied the steady flow under two intersecting wave trains in water of infinite depth. He derives the same field equations as the ones considered here; the boundary conditions are, however, different. Leibovich's model attempts to relate the Langmuir circulation to the wind at the surface where the wind stress generates a steady vorticity component $\omega^{y,s}$. In the present model, this vorticity is the result of the $O(\alpha)$ velocity fluctuations within the free surface shear layer. Leibovich attributes the Langmuir circulation to the interaction between the wind stress and the cross-stream variations of the Stokes drift. The major objection to this 'wave' model is that the intersecting waves had to be phased locked for a time much longer than the wave period, an unlikely occurrence in nature. Other models of Langmuir circulation trace the generation of the vortex rolls to an inviscid instability, with cross-stream variations, of a steady uniform flow (Craik 1977).

The model presented here suffers from the same shortcoming as the wave model: the waves have to be phase locked for a long period of time. It also provides no role for the wind, albeit for the generation of two intersecting waves. The causes of the mass transport reside solely in the wave motion: the Stokes drift in the entire flow,

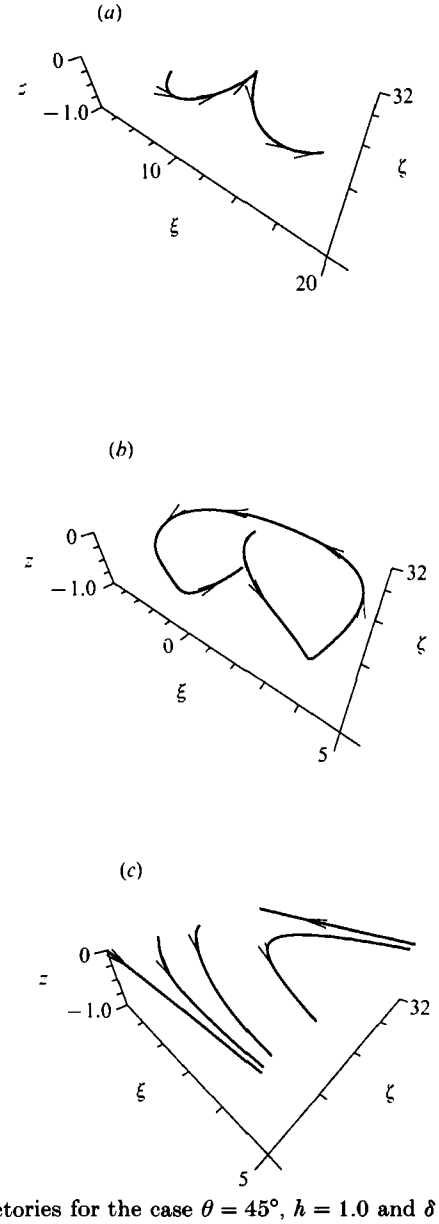

FIGURE 5. Particle trajectories for the case $\theta = 45°$, $h = 1.0$ and $\delta = 0.1$: (*a*) in the lower vortex, (*b*) in the upper vortex, and (*c*) on the surface.

the steady vorticity at the edge of the surface boundary layer, and the steady streaming at the edge of the seabed boundary layer. On the other hand, the present approach accounts explicitly for the wave motion, for the Stokes layers that develop at $O(\alpha)$ and $O(\alpha^2)$ near the seabed and the free surface, and for the presence of the seabed.

5.1. *Computational considerations*

The stability of the computations depends on the number of Chebyshev modes (L) and Fourier modes (M,N), and the choice of the time step $\Delta\tau$. This choice is a compromise between wanting a large time step to arrive to the steady solution

quickly, and the need of a small time step for a gradual development of the nonlinearities.

The number of Fourier modes kept in the computations determines the accuracy of the solution; it was hence decided to increase the number of Fourier modes until the largest magnitude of the Chebyshev coefficients, in the highest Fourier mode, is less than 10^{-6}, i.e.

$$\max_{0 \leqslant l \leqslant L} |\omega^k_{l, M, \pm N}| < 10^{-6},$$

where $k = x$, y, or z. The rate of decay of the vorticity coefficients, as the Fourier mode increases, is an indicator of the importance of the nonlinearities. These become more pronounced as the angle θ between the two waves decreases. For the case $h = 1$, and $\delta = 0.1$, the number of Fourier modes, M, had to be increased from 45 to 63 and 159 for θ equal to 45°, 30° and 15°; the time step was held constant at $\Delta\tau = 0.01$. For the case $\delta = 0.05$, 84 Fourier modes were enough to guarantee convergence; the time step was held at $\Delta\tau = 0.005$. The Chebyshev coefficients decayed at the same rate, for a fixed Fourier mode, for the three angles considered; 40 Chebyshev modes were enough to reproduce the vertical dependency of the flow.

As indicated earlier, the initial guess for the vorticity coefficients has to be solenoidal to maintain a solenoidal vorticity throughout the computations. The initial guess was chosen as a state of rest where all the coefficients are zero. This guess was then iterated until the maximum change in all Fourier–Chebyshev coefficients of the vorticity was smaller than 10^{-6},

$$\max_{0 \leqslant l \leqslant l, 0 \leqslant m \leqslant M, -N \leqslant n \leqslant N} |\omega^{k, t+1}_{l, m, n} - \omega^{k, t}_{l, m, n}| < 10^{-6}.$$

6. Mass-transport under a standing wave

In this section we consider the mass-transport under a three-dimensional standing wave. All the forcing terms are zero (Stokes drift and vorticity at free surface) except for the Eulerian streaming at the seabed. The free surface can be described by

$$\cos \kappa_x \cos \kappa_y y \cos t. \tag{64}$$

The nodes are located along the lines

$$\xi = 2\kappa_x x = k_x x = (2i+1)\pi, \quad i = 0, \pm 1, \pm 2, \ldots,$$
$$\zeta = 2\kappa_y y = k_y y = (2j+1)\pi, \quad j = 0, \pm 1, \pm 2, \ldots,$$

while the antinodes have coordinates

$$\xi = 2i\pi, \zeta = 2j\pi, \quad (i,j) = 0, \pm 1, \pm 2, \ldots.$$

The Eulerian streaming is

$$u^{\mathrm{b}} = \frac{-\kappa^3 \cos\theta}{16\beta^2 \cosh^2 \kappa h} [3\cos\zeta + (1 + 2\cos^2\theta)] \sin\xi, \tag{65}$$

$$v^{\mathrm{b}} = \frac{-\kappa^3 \sin\theta}{16\beta^2 \cosh^2 \kappa h} [3\cos\xi + (1 + 2\sin^2\theta)] \sin\zeta. \tag{66}$$

The depth and wave angle were held at $h = 1.0$ and $\theta = 45°$, while the parameter δ was given the successive values 100, 0.1, and 0.05. Only the case $\delta = 0.05$ is shown

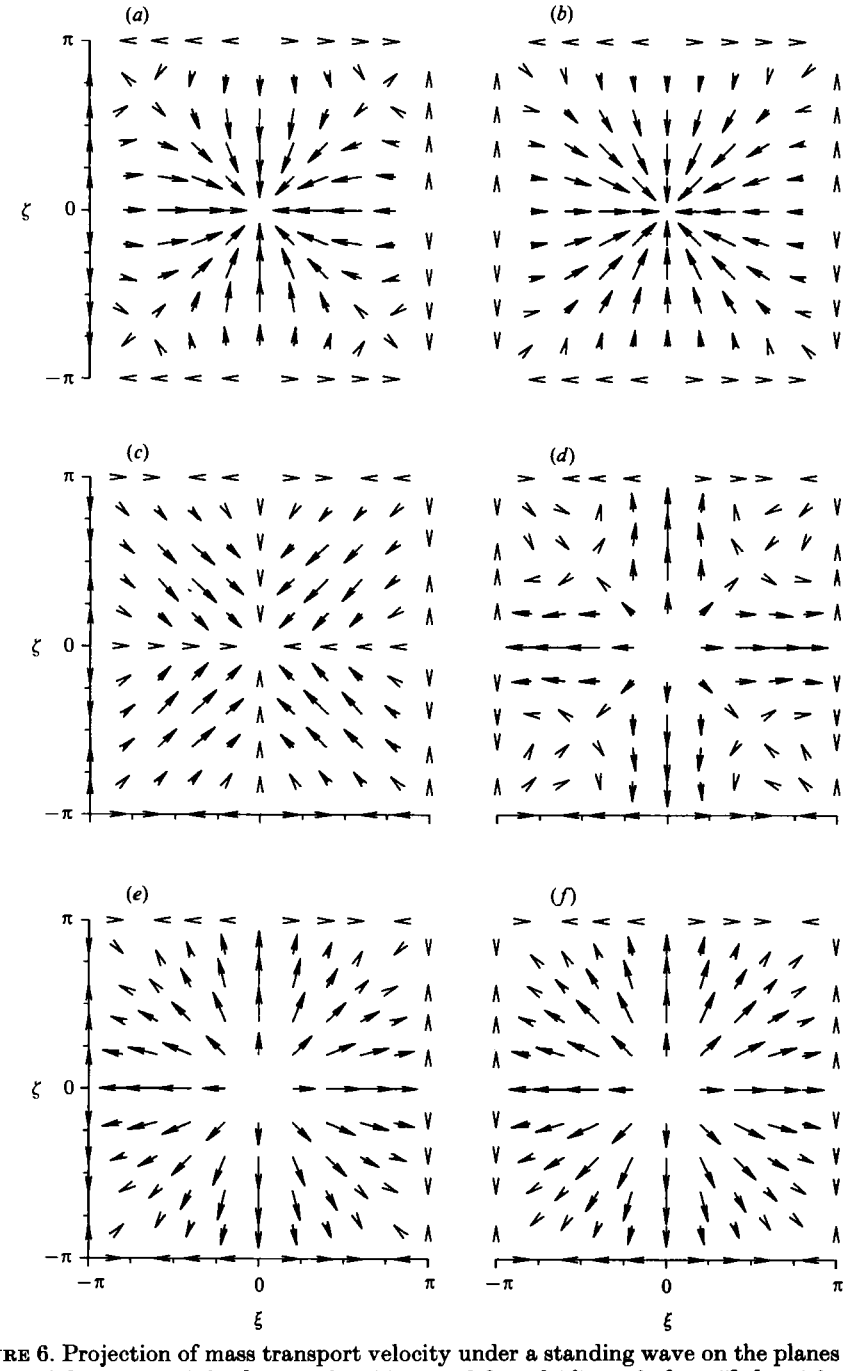

FIGURE 6. Projection of mass transport velocity under a standing wave on the planes (*a*) $z = -1.0$, (*b*) $z = -0.8$, (*c*) $z = -0.6$, (*d*) $z = -0.4$, (*e*) $z = -0.2$, and (*f*) $z = 0$. $\theta = 45°$, $h = 1.0$, and $\delta = 0.05$.

here. The highest Chebyshev mode was held at $L = 30$, while the Fourier modes (M,N) were increased from 5, to 10 and 20 as δ was decreased. The time step was also decreased with δ to stabilize the computations.

Figure 6(*a*) gives a vector diagram of the flow on the seabed. Because of the symmetry, we expect the steady flow to take place in closed cells between two

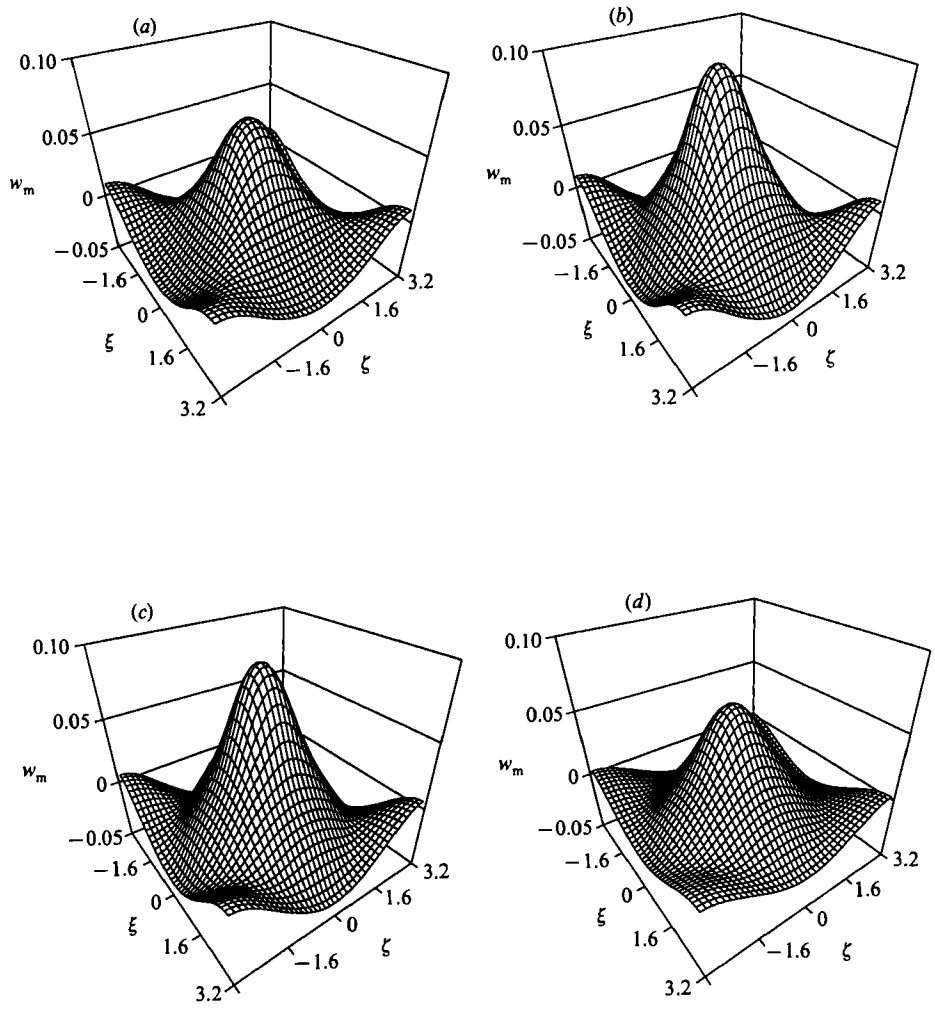

FIGURE 7. Vertical mass transport velocity at different elevation under a standing wave; $\theta = 45°$, $h = 1.0$ and $\delta = 0.05$: (*a*) $z = -0.8$, (*b*) $z = -0.6$, (*c*) $z = -0.4$, (*d*) $z = -0.2$.

consecutive nodes and antinodes in the x- and y-directions. Figure 6(*b–f*) is a series of vector diagrams of the Lagrangian velocities, u_m and v_m, at several elevations. The vertical velocity at these sections is shown in figure 7. Near the seabed, the fluid converging radially towards the antinode ($\xi = 0, \zeta = 0$) turns into an upward-shooting jet. This jet entrains fluid as it goes upward and reaches its maximum strength around mid-depth. The jet then weakens as it approaches the surface where it disappears. The flow becomes horizontal and goes towards the points ($\xi = 0$, $\zeta = \pm\pi$) and ($\xi = \pm\pi, \zeta = 0$) where it turns downward. This downward drift closes the recirculation pattern and feeds fluid into the seabed region.

Secondary circulation cells exist near the nodes ($\xi = \pm\pi, \zeta = \pm\pi$), figure 8. The upward drift in these cells is much weaker than in the jet under the antinode. The vertical velocity under the antinode increases as δ decreases, figure 9, and the

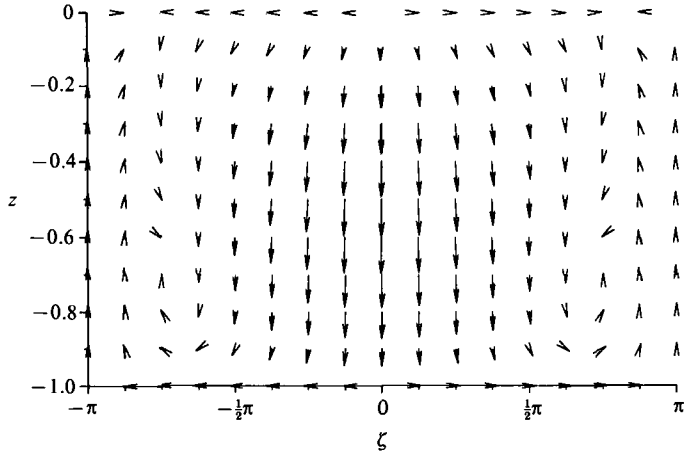

FIGURE 8. Projection of mass transport velocity under a standing wave on the plane $\xi = \pi$; $\theta = 45°$, $h = 1.0$ and $\delta = 0.05$.

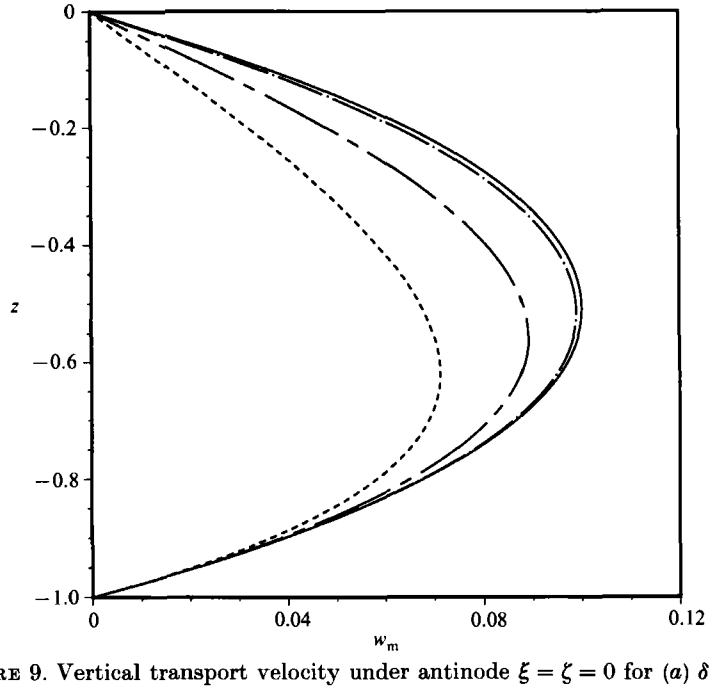

FIGURE 9. Vertical transport velocity under antinode $\xi = \zeta = 0$ for (*a*) $\delta = 0.04$ (—), (*b*) $\delta = 0.05$ (—·—), (*c*) $\delta = 0.1$ (— - —), and (*d*) $\delta = 100.0$ (----); $\xi = \pi$. $\theta = 45°$, $h = 1.0$.

location of the maximum shifts upward. Figures 10 and 11 give the vertical profile of the x-component of the velocity and vorticity vectors at $\xi = \zeta = \frac{1}{2}\pi$ for decreasing values of δ. The velocity profiles do not reveal the growth of a Stuart layer and the vertical gradient near the seabed is almost constant for the three values of δ. Only near the surface is there a noticeable change in the profile. The vorticity profile, on the other hand, shows an increase in its vertical gradient near the seabed as δ is decreased.

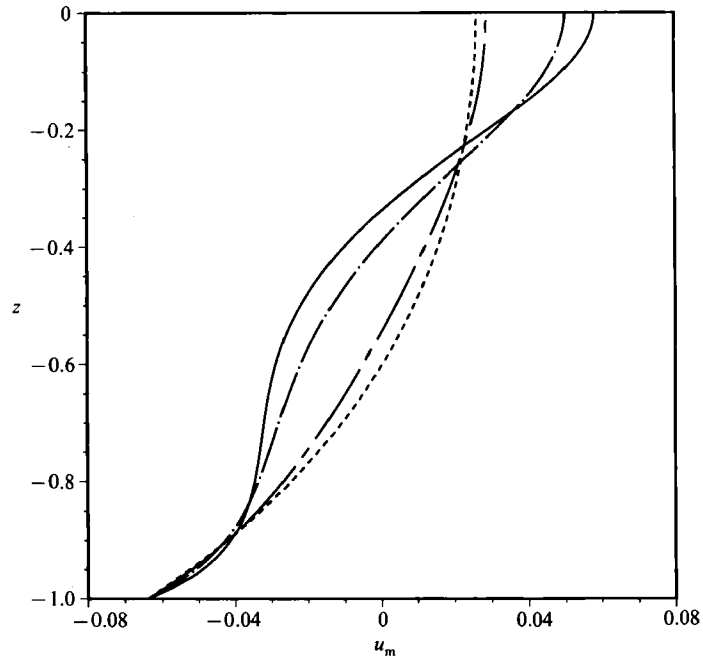

FIGURE 10. Vertical profile of mass transport velocity, u_m, at $\xi = \zeta = \frac{1}{2}\pi$ for (*a*) $\delta = 0.04$ (—), (*b*) $\delta = 0.05$ (—·—), (*c*) $\delta = 0.10$ (———), and (*d*) $\delta = 100.0$ (----). $\theta = 45°$, $h = 1.0$.

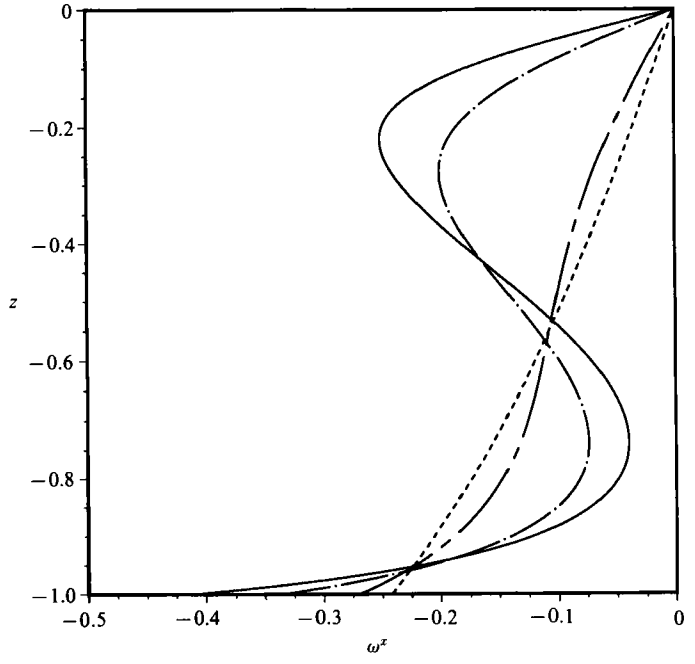

FIGURE 11. Vertical profile of vorticity, ω^x, at $\xi = \zeta = \frac{1}{2}\pi$ for (*a*) $\delta = 0.04$ (—), (*b*) $\delta = 0.05$ (—·—), (*c*) $\delta = 0.10$ (———), and (*d*) $\delta = 100.0$ (----). $\theta = 45°$, $h = 1.0$.

7. Conclusion

A Fourier–Chebyshev spectral method has been presented for the solution of the three-dimensional mass transport equations when the steady flow is periodic in two horizontal directions. The method is based on a velocity–vorticity formulation. The no-slip boundary conditions on the velocity at the seabed have been recast into two constraints on the vorticity coefficients of each Fourier mode.

The numerical solution was employed to investigate mass transport under two intersecting wave trains. The flow pattern obtained resembled the Langmuir circulation pattern. The flow depended strongly on the water depth and the parameter δ. For intermediate water depth, $h = 1.0$, the viscous solution showed the development of only one vortex. When δ was decreased to 0.1, two counter-rotating vortices appeared. Fluid in the upper vortex entrained the fluid at the surface towards the antinode. In the deep water case, $h = 3.0$, the opposite trend was seen, and only one vortex developed.

The mass transport under a three dimensional standing wave has also been computed. The solution shows the formation of a strong jet under the antinodal line, and the development of several circulation cells in the symmetry planes.

The research was supported by a grant from the National Science Foundation (CTS-8902407). Computer facilities and funds were provided by the Cornell National Supercomputer Facility (CNSF).

REFERENCES

Canuto, C., Hussaini, M. Y., Quarteroni, A. & Zang, T. A. 1988 *Spectral Methods in Fluid Dynamics*. Springer.

Craik, A. D. D. 1977 The generation of Langmuir circulations by an instability mechanism. *J. Fluid Mech.* **81**, 209–223.

Dore, B. D. 1976 Double boundary layer in standing surface waves. *Pure Appl. Geophys.* **114**, 629–637.

Fix, G. J. & Rose, M. E. 1985 A comparative study of finite element and finite difference methods for Cauchy–Riemann type equations. *SIAM J. Numer. Anal.* **22**, 250–261.

Gatski, T. B., Grosch, C. E. & Rose, M. E. 1989 The numerical solution of the Navier–Stokes equations for 3-dimensional, unsteady, incompressible flows by compact schemes. *J. Comput. Phys.* **82**, 298–329.

Gottlieb, D. & Orszag, S. A. 1977 *Numerical Analysis of Spectral Methods?: Theory and Applications*. Philadelphia: SIAM-CBMS.

Hunt, J. N. & Johns, B. 1963 Currents induced by tides and gravity waves. *Tellus* **15**, 343–351.

Iskandarani, M. 1991 Mass transport in two- and three-dimensional water waves. PhD thesis, Cornell University.

Iskandarani, M. & Liu, P. L.-F. 1991 Mass transport in two-dimensional water waves. *J. Fluid Mech.* **231**, 395–415.

Leibovich, S. 1977 On the evolution of the system of wind drift currents and Langmuir circulations in the ocean. Part 1. Theory and averaged current. *J. Fluid Mech.* **79**, 715–743.

Leibovich, S. 1983 The form and dynamics of Langmuir circulations. *Ann. Rev. Fluid Mech.* **15**, 391–427.

Liu, P. L.-F. 1977 Mass transport in the free surface boundary layer. *Coastal Engng* **1**, 207–219.

Longuet-Higgins, M. S. 1953 Mass transport in water waves. *Phil. Trans. R. Soc. Lond.* A **245**, 535–581.